La Metallurgia Italiana
International Journal of the Italian Association for Metallurgy

10.36146/2025_05_15

Experimental study of printing conditions for a NiTi alloy obtained by SLM technique

M. Gragnanini, A. Fortini, C. Morales, F. Bucchi, B. D. Monelli, G. Macoretta

The widespread adoption of additive manufacturing (AM) techniques in biomedical device production, especially with shape memory materials like NiTi alloys, is well-established due to their unique properties.
However, traditional manufacturing techniques face limitations when working with these alloys, prompting high interest in AM research, with a special focus on the Selective Laser Melting (SLM) technique. In this study, a comprehensive analysis of the printing conditions for NiTi alloys depositions through the SLM technique was conducted. With the support of a previously explored analytical approach, experimental trials were designed to investigate the printability of the NiTi alloy. NiTi samples were produced using an SLM machine with a maximum laser power of 500 W, operating in continuous mode (also called pulsed), and with two different layer thicknesses, i.e. 30 μm and 60 μm. Experimental analyses, including optical and electron microscopy were carried out to assess the microstructural characteristics of the printed samples. Our findings enabled a preliminary exploration of the material's printability.

KEYWORDS: ADDITIVE MANUFACTURING, NITI ALLOYS, FULL FACTORIAL DESIGN OF EXPERIMENT, MICROSTRUCTURE, PSEUDOELASTICITY;

INTRODUCTION

Additive manufacturing, also known as 3D printing, has garnered significant attention in recent decades in both research and production environments as an effective alternative to conventional methods for manufacturing components in the automotive, aerospace, and biomedical sectors. This is due to its numerous advantages, including cost reduction, customization, geometric complexity, and the ability to print a wide range of materials, such as NiTi alloys [1] [2], [3]. These alloys, as part of the shape memory alloy family, can convert thermal energy into mechanical work, which promotes them widely employed for engineering applications [4], [5]. Furthermore, these materials exhibit exceptional properties such as pseudoelasticity, inherent biocompatibility, and corrosion resistance [6]. In order to fully exploit these material properties and overcome challenges such as poor machinability, oxygen contamination risk [7], and high compositional sensitivity [8], AM technologies have been explored in recent years, particularly the Selective Laser Melting (SLM) technique, to produce shape memory alloy parts [9]. In the present work, the feasibility of printing NiTi samples using the

M. Gragnanini, A. Fortini, C. Morales
Università di Ferrara, Dipartimento di Ingegneria

F. Bucchi, B. D. Monelli, G. Macoretta
Università di Pisa, Dipartimento di Ingegneria Civile e Industriale
michele.gragnanini@unife.it

SLM technique was investigated based on the results of an analytical model, developed from a thermal field produced by the laser heat source under steady-state conditions, and from insights based on literature analysis. Experimental analyses conducted on the samples allowed for the identification of the material's feasible region.

BIBLIOGRAPHIC ANALYSIS: SLM and NiTi ALLOYS

The Selective Laser Melting (SLM) technique involves the use of a high-power laser to melt and fuse metal powders in a layer-by-layer process to create 3D near-net-shape structures [1], [2]. When this technology is applied to materials such as NiTi alloys, the printing process is referred to as 4D printing [2] because it enables the production of components with complex and functional geometries that change their shape or mechanical response depending on temperature variations. The synergy between the unique properties of NiTi and the precision of the SLM technique brings remarkable innovation for applications requiring complex, highly engineered designs, such as biomedical implants and aerospace components [3]. The SLM process parameters play a critical role in determining the quality of the final component, as even slight variations can significantly impact the resulting microstructure, affecting aspects like grain size, constituents, and defect formation. Additionally, in the case of NiTi, these variations can alter the alloy's transformation temperatures [6]. As shown in Fig. 1, numerous parameters affect the SLM process and can be grouped into broad categories based on their relationship with the main process factors [7]. However, the most important distinction is between predefined and controllable parameters. Specifically, the predefined parameters are the ones that depend on the powder's size and morphology, the component's geometry, and the printing environment [9]. Meanwhile, the controllable parameters can be adjusted during the printing process.

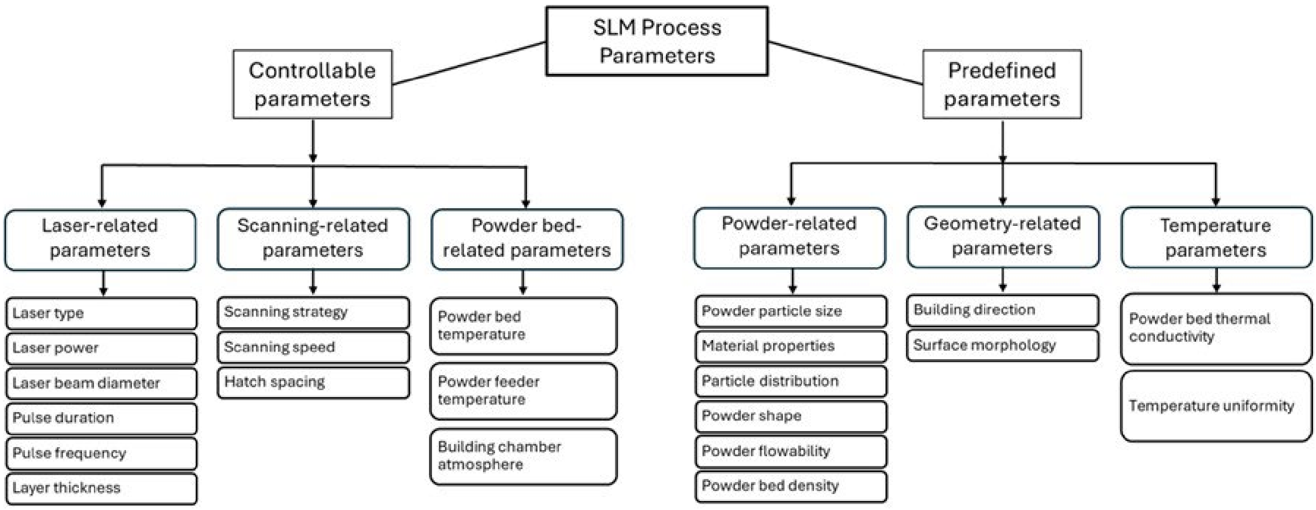

Fig.1 - Controllable and predefined parameters of the SLM process. Adapted from [7].

Among all the controllable parameters, the most extensively investigated in the literature are Laser power (P), scanning speed (V_S), hatch spacing (H_S) and layer thickness (t). Laser power (P), measured in W, refers to the laser's energy output per unit of time and determines the extent of melting in the powder bed. Adequate laser power ensures sufficient energy to achieve proper melting and bonding of the metal powders, which is essential for a dense and high-quality structure. However, excessive laser power can lead to defects such as keyhole porosity, spatter, and thermal cracking due to overheating and excessive melting. Scanning speed (V_S), typically measured in mm/s, is the rate at which the laser moves across the powder bed, controlling energy distribution where slower speeds create larger melt pools and stronger bonding. Hatch spacing (H_S), the distance between adjacent laser scan lines, influences layer uniformity by controlling overlap between passes; too large a spacing may create unmelted areas, while too small a spacing can cause overheating. Finally, layer thickness (t), defined as the height of each powder layer, determines the resolution and build speed, where thinner layers enhance detail but increase print time, while thicker layers allow faster builds but may reduce precision. Table I summarizes the most common value ranges for P, V_S, H_S, and t for the printing of NiTi components according to [3], [6], with their graphical definition shown in Fig. 2 [3], [8]. These values can be adopted to compute the energy density (E_D) parameter, defined by Eq. (1) as follows:

$$E_D = \frac{P}{V_S \times t \times H_S} \tag{1}$$

To achieve characteristics that meet the required specifications, a deep understanding of the process parameters and how they influence the onset of defects during printing is required [3], [10], [11], [12], [13], [14], [15]. The most common defects associated with the printing of NiTi components are the presence of impurities, excessive surface roughness, fractures, keyholes, and lack of fusion (LOF) [9]. Impurities, primarily oxygen and carbon, play a key role in achieving a fully dense component. Rapid heating and cooling cycles promote the growth of intermetallic phases ($TiNi_3$/Ti_2Ni) and oxides (Ti_4Ni_2O), which generate porosity, negatively impacting the mechanical properties and altering the alloy's transition temperatures [16].

Parameters that directly affect impurity absorption include energy density and powder granulometry. It has been observed that impurity absorption increases dramatically when the energy density exceeds 200 J/mm3, and particles with a granulometry of 45–100 µm show less tendency for oxygen absorption compared to smaller particles [14], [17], [18]. Surface roughness, a central concern in biomedical implants, is strongly dependent on the process's energy density and is negatively affected by the sintering of partially melted particles adhering to the component's surfaces [19]. Specifically, it has been observed that for the printing of NiTi components, the lowest roughness values are achieved with approximately 43 J/mm3 [18]. Crack formation is primarily attributed to different cooling rates, phase transformations related to excessive thermal stress, delamination in areas characterized by lack of fusion, and residual stress. The process parameter that most influences crack formation is the scanning speed. Excessively high scanning speeds (over 1000 m/s)
can lead to too rapid cooling rates, promoting the formation of a brittle intermetallic phase (Ti_2Ni) between the layers, which serves as a preferential site for crack formation [9], [20]. Keyholes and lack of fusion depend on laser power, which determines penetration depth. In the case of keyholes, excessive penetration results in the formation of cavities with variable geometry within the component [21], while lack of fusion is caused by low laser power (50–100 W), which, when combined with excessively high scanning speeds, leads to insufficient penetration. This results in partially melted powder being trapped inside the component, significantly worsening its fatigue behavior [8], [21]. Considering the challenges and defects that can be introduced during SLM of NiTi components, an analytical study was conducted to define the printable region for the Ni50.8Ti49.2 alloy, aiming to produce defect-free samples.

Tab.1 - Controllable parameters [9].

Laser power (P)	15 – 200 (W)
Scanning speed (VS)	200 – 1200 (mm/s)
Hatch spacing (HS)	60 – 100 (µm)
Layer thickness (t)	20 – 100 (µm)

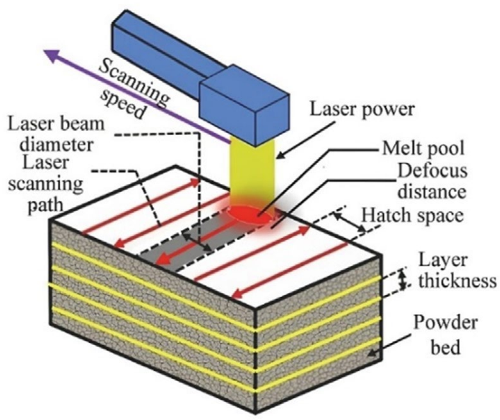

Fig.2 - Controllable parameters [9].

EXPERIMENTAL STUDY

NiTi powder produced by gas atomization in an Ar atmosphere was used. The as-received powder was analyzed by a Zeiss EVO MA15 (Carl Zeiss, Jena, Germany) scanning electron microscope (SEM). Due to this production technique, the powder exhibits a spherical morphology, as visible in the SEM images in Fig. 3. Based on the particle size analysis provided by the supplier, the powder has diameters ranging from 13 μm to 53 μm (D10-D90).

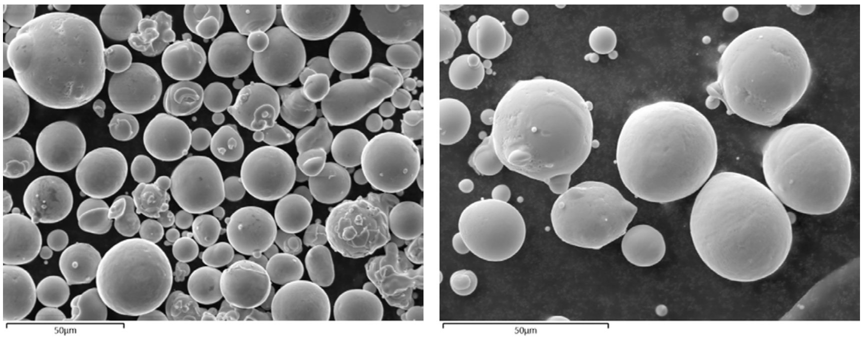

(a) (b)

Fig.3 - SEM images of the adopted NiTi powder.

The specimens were produced using the Renishaw RenAM500S Flex (Renishaw, Wotton-under-Edge, United Kingdom) printer installed at the Metal Additive Manufacturing Laboratory of the University of Pisa, equipped with a volume reduction accessory (Reduction Build Volume). This accessory allows a print volume reduction to a cube with dimensions of 80 mm x 80 mm x 50 mm. As a result, a reduced amount of powder, approximately 1 kg, was used. The samples were fabricated in a vertical orientation, with the largest dimension aligned along the building direction. To prevent oxidation during printing, the chamber was filled with Ar, ensuring an O_2 presence of less than 20 ppm during the process. The specimens were printed on a Ti alloy (Ti6Al4V) substrate. A wide set of SLM process parameters featuring energy density values ranging between 21.7 and 185 J/mm^3, was defined on the basis of the values adopted in recent literature studies that employed a powder with the same composition as that used in this study [26], [27], [28], [29], [30], [31]. Only the process parameters that produced a material with nonlinear elasticity properties were selected. Based on these energy density values, 10 combinations of power, scanning speed, layer thickness, and hatch distance were defined, aimed at exploring the limits of the printability region and the effects of process parameters on the microstructural properties of the material. The explored ED values are reported in Tab II. Once an ED value was selected, the process parameters were determined based on an analytical model that extended Rosenthal's solution to the SLM process [22], [23]. The model is aimed at increasing the process efficiency, avoiding the onset of macroscopic defects such as LOFs and keyhole-induced porosity, as demonstrated by Macoretta et al. in previous studies [24], [25]. The layer thickness was set to either 30 μm or 60 μm, while the scanning speed, laser power and hatch distance varied within a range of 0.3 to 1.75 m/s, 65 to 450 W and 30 to 120 μm, respectively. The laser was operated in continuous wave mode. Samples 9 and 10 were aimed at investigating the lower ED boundary, where the occurrence of LOF defects can be predicted by the analytical model. A cubic sample with a side length of 5 mm and a height of 3.5 mm, parallel to the building direction (BD), was printed per each investigated process parameter. The samples featured a pyramidal base to facilitate secure attachment to the build plate. A representative image, taken with the Hirox HRX-01 (Hirox, Tokyo, Japan) digital 3D optical microscope is shown in Fig. 4. Microstructural analysis and image analysis for the determination of porosity percentage were conducted on all SLM-printed samples after standard metallographic preparation, which included cutting, resin embedding, grinding, polishing, and metallographic etching with Kroll's reagent (92 % H_2O, 5 % HNO_3, 3 % HF). Observations were made using a Leica DMi 8 A optical microscope (OM) (Leica, Wetzlar, Germany) and with the previously mentioned SEM microscope, while image analysis was conducted using Image J software (Image J, Maryland, US). The porosity percentage, evaluated on 10 micrographs at 200x magnification randomly acquired on the analyzed surfaces, was computed as the ratio of the pore surface to the total analyzed surface.

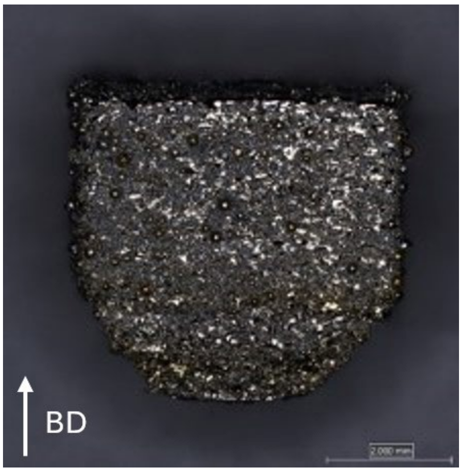

Fig.4 - Representative image of an SLM printed sample.

Tab. 2 - Energy density (ED) values used for sample printing.

Sample name	E_D [J/mm3]
1	185.2
2	185.2
3	83.3
4	82.4
5	55.6
6	55.6
7	55.6
8	54.9
9	35.0
10	21.7

RESULTS AND DISCUSSION

The results of the image analysis are reported in the plot of Fig. 5, which displays the porosity percentage as a function of the investigated sample. As seen, the combination of printing parameters and the resulting energy density used allows the production of dense samples with porosity percentages below 0.5 % for samples 1, 2, 3, 5, and 7 and below 1 % for samples 6 and 8. As shown in the graph, samples 9 and 10, printed with low energy density values, used to explore the LOF region, displayed relatively high porosity percentages. Sample 9 exhibited a porosity percentage above 3.5 %, while sample 10 showed excessive porosity levels that were not measured. Conversely, sample 4, printed with the same energy density values as sample 3, highlights that its ED value is insufficient to achieve acceptable density. Therefore, the variation of individual parameters plays a significant role and cannot be disregarded.

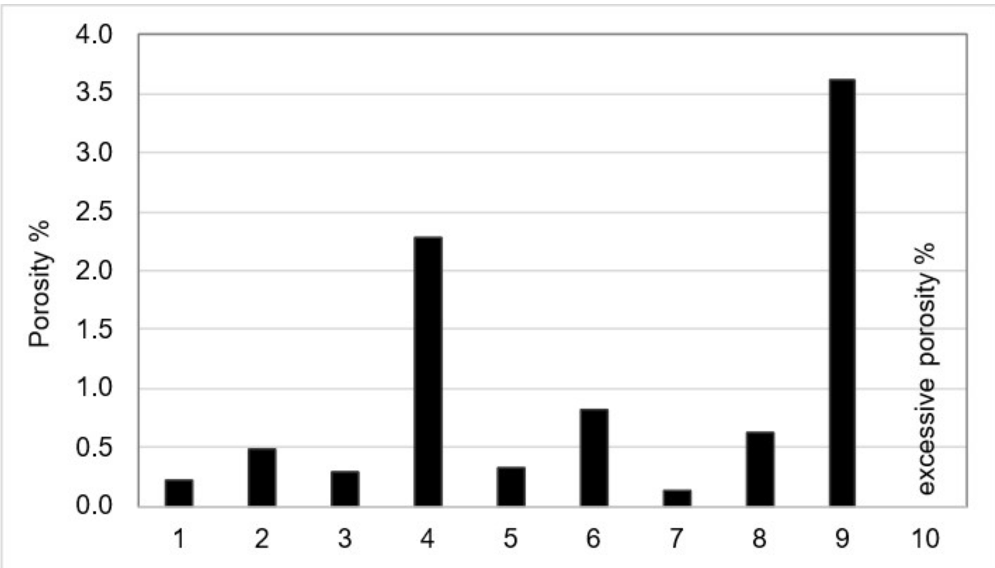

Fig.5 - Results of the image analysis in decreasing order of E_D.

According to the results of the image analysis, metallographic observation of the specimens revealed the presence of defects such as LOF, highlighted with white arrows in the sample 9 micrograph showed in Fig. 6a). Besides the keyhole phenomena depicted in sample 4 micrograph 4 in Fig. 6b), highlighted by red arrows.

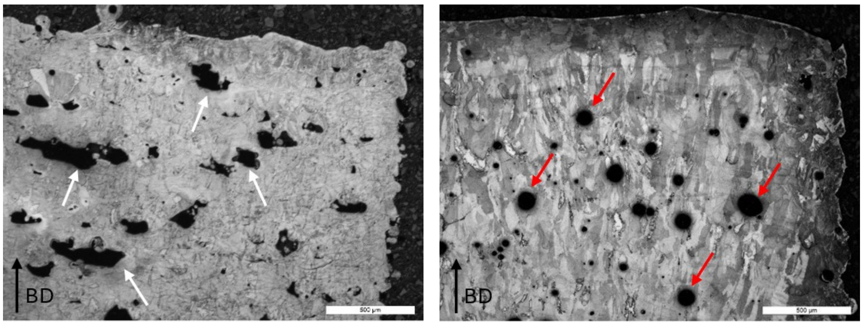

(a) (b)

Fig.6 - OM micrographs of: a) sample 9 with widespread LOF defects, E_D 35 J/mm³; b) sample 4 with widespread keyhole defects, E_D 82.4 J/mm³.

Fig. 7a) and Fig. 7b) depict the OM micrographs of samples 7 and 1, respectively. A compact structure almost free of defects, consisting of columnar grains parallel to the build direction is shown highlighted by the black boxes. The analysis allowed for the preliminary identification of a printability region where the material is unaffected by repeatable macroscopic defects and achieves an average density, which was calculated by subtracting the measured porosity percentage from the total area of the sample, resulting in a 99.8 % and 99.9 % for specimens 1 and 7, respectively.

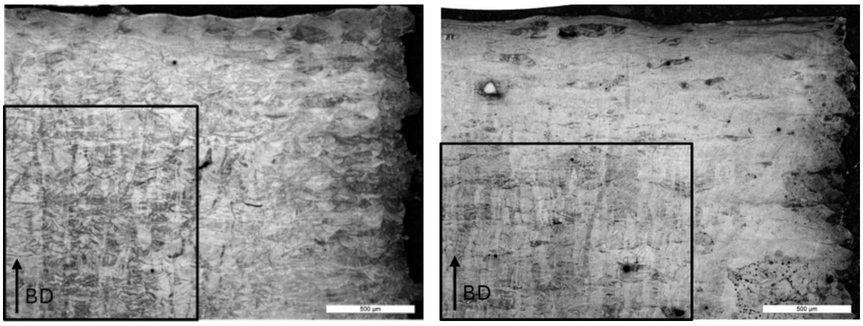

(a) (b)

Fig.7 - OM micrographs of samples with a compact structure almost defects-free: a) sample 7, ED 55.6 J/mm³ b) sample 1 ED 185.2 J/mm³ .

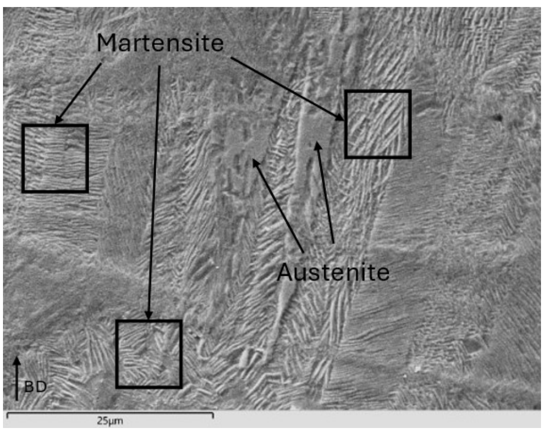

Fig.8 - Secondary electron SEM micrograph of sample 7.

CONCLUSIONS

Based on the analytical modeling of the non-dimensionalized printability region using selective laser melting (SLM) technology for the $Ni_{50.8}Ti_{49.2}$ alloy, 10 combinations of process parameters, including laser power, scanning speed, hatch distance, layer thickness were defined for a preliminary exploration of the material's printability. Metallographic analyses were conducted to determine the defects introduced by the printing process, which enabled for the identification of 5 parameter combinations with porosity < 0.5 % and of 2 parameter combinations with porosity < 1 %. The study allowed for the identification of an energy density threshold below which LOF occurs, negatively affecting the material's porosity. This result led to the identification of a preliminary printability region for the adopted material.

ACKNOWLEDGMENTS

The authors would like to thank Alberto Coda for his operational support and valuable advice regarding the material printing process, and Ottavia Vezzani for her operational assistance in the metallographic preparation of the samples.

FOUNDING

Progetto PRIN 2022 "20228AZTYB - GIFTED (desiGn of addItive manuFactured niTinol Endovascular Devices)" - Finanziamento UE - NextGenEU - M4C2, Inv.1.1 - CUP: F53D23001630006

REFERENCES

[1] D. Srinivasan et al., "3D Printing Manufacturing Techniques, Materials, and Applications: An Overview," 2021, Hindawi Limited. doi: 10.1155/2021/5756563.

[2] Z. X. Khoo, Y. Liu, J. An, C. K. Chua, Y. F. Shen, and C. N. Kuo, "A review of selective laser melted NiTi shape memory alloy," Mar. 29, 2018, MDPI AG. doi: 10.3390/ma11040519.

[3] X. Wang et al., "Effect of process parameters on the phase transformation behavior and tensile properties of NiTi shape memory alloys fabricated by selective laser melting," Addit Manuf, vol. 36, Dec. 2020, doi: 10.1016/j.addma.2020.101545.

[4] A. Suman, E. Fabbri, A. Fortini, M. Merlin, and M. Pinelli, "On the design strategies for SMA-based morphing actuators: state of the art and common practices applied to a fascinating case study," Nov. 01, 2020, SAGE Publications Ltd. doi: 10.1177/0954410020925687.

[5] A. Suman, A. Fortini, N. Aldi, M. Merlin, and M. Pinelli, "A Shape Memory Alloy-Based Morphing Axial Fan Blade-Part II: Blade Shape and Computational Fluid Dynamics Analyses," J Eng Gas Turbine Power, vol. 138, no. 6, Jun. 2016, doi: 10.1115/1.4031760.

[6] M. Speirs et al., "On the Transformation Behavior of NiTi Shape-Memory Alloy Produced by SLM," Shape Memory and Superelasticity, vol. 2, no. 4, pp. 310–316, Dec. 2016, doi: 10.1007/s40830-016-0083-y.

[7] A. S. Metel, M. M. Stebulyanin, S. V. Fedorov, and A. A. Okunkova, "Power Density Distribution for Laser Additive Manufacturing (SLM): Potential, Fundamentals and Advanced Applications," Technologies (Basel), vol. 7, no. 1, Mar. 2019, doi: 10.3390/technologies7010005.

[8] S. Dadbakhsh, M. Speirs, J. P. Kruth, J. Schrooten, J. Luyten, and J. Van Humbeeck, "Effect of SLM parameters on transformation temperatures of shape memory nickel titanium parts," Adv Eng Mater, vol. 16, no. 9, pp. 1140–1146, Sep. 2014, doi: 10.1002/adem.201300558.

[9] O. A. Mohamed, S. H. Masood, and W. Xu, "Nickel-titanium shape memory alloys made by selective laser melting: a review on process optimisation," Adv Manuf, vol. 10, no. 1, pp. 24–58, Mar. 2022, doi: 10.1007/s40436-021-00376-9.

[10] M. H. Elahinia, M. Hashemi, M. Tabesh, and S. B. Bhaduri, "Manufacturing and processing of NiTi implants: A review," 2012, Elsevier Ltd. doi: 10.1016/j.pmatsci.2011.11.001.

[11] S. Ehsan Saghaian et al., "Effect of hatch spacing and laser power on microstructure, texture, and thermomechanical properties of laser powder bed fusion (L-PBF) additively manufactured NiTi," Opt Laser Technol, vol. 149, May 2022, doi: 10.1016/j.optlastec.2021.107680.

[12] M. De Wild, F. Meier, T. Bormann, C. B. C. Howald, and B. Müller, "Damping of selective-laser-melted NiTi for medical implants," in Journal of Materials Engineering and Performance, Springer New York LLC, 2014, pp. 2614–2619. doi: 10.1007/s11665-014-0889-8.

[13] C. A. Biffi, J. Fiocchi, F. Valenza, P. Bassani, and A. Tuissi, "Selective Laser Melting of NiTi Shape Memory Alloy: Processability, Microstructure, and Superelasticity," Shape Memory and Superelasticity, vol. 6, no. 3, pp. 342–353, Sep. 2020, doi: 10.1007/s40830-020-00298-8.

[14] S. F. Ou, B. Y. Peng, Y. C. Chen, and M. H. Tsai, "Manufacturing and characterization of NiTi alloy with functional properties by selective laser melting," Metals (Basel), vol. 8, no. 5, May 2018, doi: 10.3390/met8050342.
[15] T. Bormann, B. Müller, M. Schinhammer, A. Kessler, P. Thalmann, and M. De Wild, "Microstructure of selective laser melted nickel-titanium," Mater Charact, vol. 94, pp. 189–202, 2014, doi: 10.1016/j.matchar.2014.05.017.
[16] Z. Yu et al., "Prediction of SLM-NiTi transition temperatures based on improved Levenberg–Marquardt algorithm," Journal of Materials Research and Technology, vol. 15, pp. 3349–3356, Nov. 2021, doi: 10.1016/j.jmrt.2021.09.149.
[17] J. M. Walker, C. Haberland, M. Taheri Andani, H. E. Karaca, D. Dean, and M. Elahinia, "Process development and characterization of additively manufactured nickel–titanium shape memory parts," J Intell Mater Syst Struct, vol. 27, no. 19, pp. 2653–2660, Mar. 2016, doi: 10.1177/1045389X16635848.
[18] C. Haberland, M. Elahinia, J. M. Walker, H. Meier, and J. Frenzel, "On the development of high quality NiTi shape memory and pseudoelastic parts by additive manufacturing," Smart Mater Struct, vol. 23, no. 10, p. 104002, Sep. 2014, doi: 10.1088/0964-1726/23/10/104002.
[19] A. Domashenkov, M. Doubenskaia, I. Smurov, M. Smirnov, and A. Travianov, "Selective laser melting of NiTi powder Maria Doubenskaia École nationale d'ingénieurs de Saint-Étienne I. Smurov École nationale d'ingénieurs de Saint-Étienne Selective laser melting of NiTi powder," 2017. [Online]. Available: https://www.researchgate.net/publication/361446736
[20] H. L. Baker, "The Development and Processing of Nickel Titanium Shape Memory Alloys Containing Palladium using Selective Laser Melting," 2018.
[21] C. Wang et al., "Additive manufacturing of NiTi shape memory alloys using pre-mixed powders," J Mater Process Technol, vol. 271, pp. 152–161, Sep. 2019, doi: 10.1016/j.jmatprotec.2019.03.025.
[22] Rosenthal D., The Theory of Moving Sources of Heat and Its Application to Metal Treatments. Transactions ASME 1946;43:849–66.
[23] M. Moda, A. Chiocca, G. Macoretta, B. D. Monelli, and L. Bertini, "Technological implications of the Rosenthal solution for a moving point heat source in steady state on a semi-infinite solid," Mater Des, vol. 223, Nov. 2022, doi: 10.1016/j.matdes.2022.110991.
[24] G. Macoretta, L. Bertini, B. D. Monelli, and F. Berto, "Productivity-oriented SLM process parameters effect on the fatigue strength of Inconel 718," Int J Fatigue, vol. 168, Mar. 2023, doi: 10.1016/j.ijfatigue.2022.107384.
[25] M. Abruzzo, G. Macoretta, B. D. Monelli, and L. Romoli, "Impact of process parameters on the dynamic behavior of Inconel 718 fabricated via laser powder bed fusion," International Journal of Advanced Manufacturing Technology, vol. 132, no. 7–8, pp. 3655–3669, Jun. 2024, doi: 10.1007/s00170-024-13526-7.
[26] A. Safdel, H. Torbati-Sarraf, and M. A. Elbestawi, "Laser powder bed fusion of differently designed NiTi stent structures having enhanced recoverability and superelasticity," J Alloys Compd, vol. 954, Sep. 2023, doi: 10.1016/j.jallcom.2023.170196.
[27] J. N. Zhu, E. Borisov, X. Liang, E. Farber, M. J. M. Hermans, and V. A. Popovich, "Predictive analytical modelling and experimental validation of processing maps in additive manufacturing of nitinol alloys," Addit Manuf, vol. 38, Feb. 2021, doi: 10.1016/j.addma.2020.101802.
[28] V. Finazzi, F. Berti, L. Petrini, B. Previtali, and A. G. Demir, "Additive manufacturing and post-processing of superelastic NiTi micro struts as building blocks for cardiovascular stents," Addit Manuf, vol. 70, May 2023, doi: 10.1016/j.addma.2023.103561.
[29] M. Nematollahi, K. Safaei, P. Bayati, and M. Elahinia, "Functionally graded NiTi shape memory alloy: Selective laser melting fabrication and multi-scale characterization," Mater Lett, vol. 292, Jun. 2021, doi: 10.1016/j.matlet.2021.129648.
[30] C. A. Biffi, P. Bassani, J. Fiocchi, and A. Tuissi, "Microstructural and mechanical response of niti lattice 3d structure produced by selective laser melting," Metals (Basel), vol. 10, no. 6, pp. 1–9, Jun. 2020, doi: 10.3390/met10060814.
[31] N. Shayesteh Moghaddam et al., "Achieving superelasticity in additively manufactured NiTi in compression without post-process heat treatment," Sci Rep, vol. 9, no. 1, Dec. 2019, doi: 10.1038/s41598-018-36641-4.
[32] C. H. Fu, M. P. Sealy, Y. B. Guo, and X. T. Wei, "Austenite-martensite phase transformation of biomedical Nitinol by ball burnishing," J Mater Process Technol, vol. 214, no. 12, pp. 3122–3130, 2014, doi: 10.1016/j.jmatprotec.2014.07.019.

TORNA ALL'INDICE >